33rd Annual International Conference of the IEEE EMBS
Boston, Massachusetts USA, August 30 - September 3, 2011

Automatic extraction of sulcal lines on the cortical surface using shortest path probability maps

Arnaud Le Troter, Guillaume Auzias, Olivier Coulon

***Abstract*— This paper describes an automatic procedure for extracting sulcal lines from cortical surface meshes of the human brain, which will serve as a tool for landmark extraction as well as for investigating the morphometry of sulci. The procedure consists in a sequence of steps, including sulcal basin segmentation based on local curvature information, estimating a bundle of depth-constrained geodesic paths and determining a robust probability map of sulcal lines crossing. In this experiment, we present quantitative validations on two main sulci to observe the agreement of our method with manually traced curves.**

I. INTRODUCTION

A growing number of methods for analysing cortical anatomical and/or functional data rely on the extraction of cortical folding patterns. For example in the context of inter-subject brain registration, sulcal landmarks are used to constraint the parameterization of the cortical surface [1] and enforce the correspondance between indivuals. The accuracy and robustness of these landmarks is therefore essential but the manual delineation of sulcal lines is a difficult and time-consuming task ([2], [3], [4]) .

Indeed, several approaches for the automatic extraction of sulcal fundi from the cortical surface has been proposed [1], [5], [6], [7], [8]. The Brainvisa[1] software provides methods for the identification [9] and projection [10] of main sulci on the cortical surface. The resulting projected sulci show several components and branches that are not anatomically relevant and should therefore not be considered as landmarks. Clouchoux et al. [1] propose a procedure to transform each sulcal projection into a single smooth line without branche using a multi-resolution snake algorithm. However, the reduction of sulcal fundi to a single line is not always justified since for sulci with multiple compartments the resulting sulcal line would cross a gyrus. Furthermore, this method does not always provide the expected quality (lack of accuracy, wrong connectivity).

In this paper we present a new method that performs an automatic and robust sulcal line extraction, and aims at finding a single line per sulcal basins. It is based on a geodesic distance constrained by the cortical geometry (curvature, depth) and the definition of a shortest path probability map within each sulcal basin. In the next section we present our algorithm then in section 3 we evaluate the process on a set of 20 subjects.

All authors are with Laboratoire des Sciences de l'Information et des Systèmes, UMR CNRS 6168, Marseille, France arnaud.le-troter@univmed.fr

[1]http://brainvisa.info

II. METHODS

Individual cortical surfaces are extracted from T1-weighted images. Discrete curvature and geodesic depth maps are estimated from each mesh using Brainvisa (see "Fig. 1(a)" and "Fig. 1(b)"). These methods are described in detail by Cachia [10]. The cortical tiangular mesh, denoted as M, is composed of n vertices $V = \{v_1, v_2, \ldots, v_n\}$, and m edges $E = \{e_1, e_2, \ldots, e_m\}$. Each vertex $v_i \in V$ is a point in 3D space $v_i = (x_i, y_i, z_i)$ and each edge $e_k \in E$ connects together a pair of vertices (v_i, v_j).

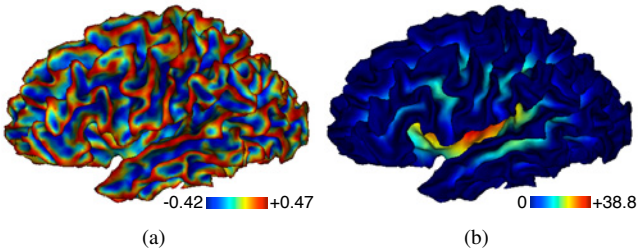

Fig. 1. The discrete curvature map (a), the geodesic depth map (b) and the cortical mesh are computed using Brainvisa.

In [4], Shattuck et al. describe a semi-automated curve tracking algorithm for the delineation of sulci on the cortical surface. This method computes the shortest path constrained by curvature between any two given extremity vertices. We extend this approach in order to obtain a fully automatic sulcal extraction as follows:

1) the geodesic paths are constrained by the depth map instead of a local measure of convexity (similar to a computation of mean curvature), because we observed that it leads to a better definition of sulcal lines.
2) the two extremities of each sulcal line are identified automatically.

As the estimation of shortest paths is essential in our approach, we briefly describe this step (more details can be found in [4]).

A. Geodesics, Shortest Paths and Weighted Graphs

A geodesic path is composed of a set of points on the cortical surface mesh linked by edges. Let us consider the cortical mesh as a weighted graph $G = (E, V, W)$. The paths between any pair of vertices is obtained using Dijkstra's algorithm [11], [12]. The algorithm finds the path with lowest weight (i.e. the shortest path) between a given source vertex in the mesh and any other vertex. Sulcal lines can thus be defined as shortest paths in the weighted graph with

appropriate weighting. The weight $w_k \in W$ associated to the edge e_k is defined as :

$$w_k = (\alpha_i + \alpha_j).\|v_i - v_j\| \quad (1)$$

where α_i is a cost function associated to the vertex v_i:

$$\alpha_i = \left(\frac{1}{1 + exp^{\lambda.c_i}}\right)^{\gamma} \text{, as defined in [4]} \quad (2)$$

Contrary to the authors of [4] who proposed to use a local measure of convexity at the vertex v_i for c_i, we suggest to take advantage of the geodesic depth (See "Fig. 3(b)") as described in next section. λ and γ are two parameters that balance the influence of the cost function versus the length of the edge in w_k "(1)". We empirically fixed $\lambda = 3$ and $\gamma = 2$ to obtain geodesic paths that properly follow the fundus of the sulci.

The path that connects the vertices v_i and v_j is then defined as P_{ij}. The weighted length L of a path P_{ij} is the sum of the weights of the edges forming the path connecting the two vertices:

$$L(P_{ij}) = \sum_{w_k | e_k \in P_{ij}} w_k \quad (3)$$

and S_{ij} is the shortest path among all possible paths, whose length is minimal.

$$S_{ij} = \arg\min(L(P_{ij})) \quad (4)$$

"Fig. 2" shows an example of a sulcal line resulting from the depth-constrained shortest path on a cortical surface.

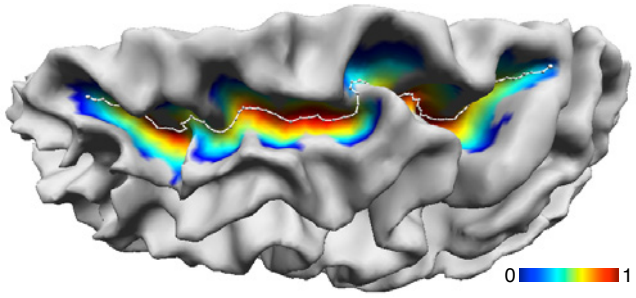

Fig. 2. The depth map for the superior frontal sulcus is shown as a colored texture (deeper parts in red). The shortest path constrained by this depth map is shown as a white line.

B. Automatic identification of sulcal lines extremities

We introduce a new method to automatically and robustely identify the extremities of the sulcal lines that will be linked by the shortest path as defined in previous section. In order to avoid gyrus crossing, it seems logical to separate the basins and the ridges. This separation is a process of segmentation and define the regions of interest (sulcal basins) in which we seek sulcal lines. The first idea is that ridges and basins have opposite curvature signs.

1) Segmentation of sulcal basins: Boundaries between basins are either saddles or ridges and have positive or zero curvature value. First, we threshold discrete curvature map by keeping only the negative curvature ("Fig. 1(a)") followed by a morphological closing to reduce noise. A connected components algorithm is then applied and results in a set of sulcal basins as illustrated on "Fig. 3(a)". Let us denote $B \subset V$ the set of resulting sulcal basins. In each sulcal basin the depth is then normalized to vary between 0 and 1 ("Fig. 3(b)").

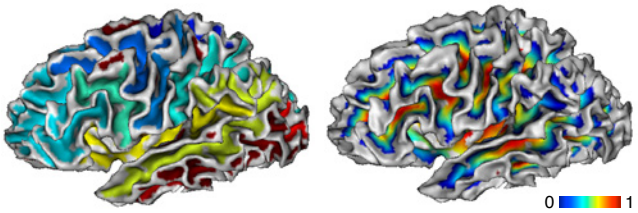

(a) (b)

Fig. 3. (a) labelled sulcal basins B (b) normalized geodesic depth map by basin

We then consider the projection of main bottom sulcal lines on triangulated cortical surfaces [10]. This projection results in a complex sulcal representation to which is associated a label corresponding to the sulcus nomenclature.

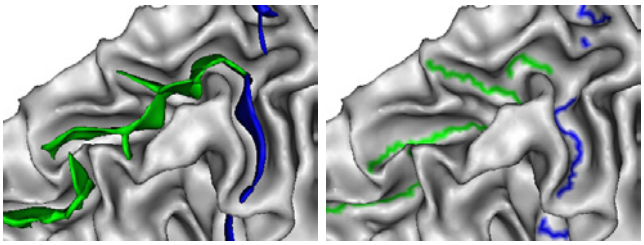

(a) (b)

Fig. 4. (a) Identification of sulci (b) Projections of bottom lines

These two steps of identification ("Fig. 4(a)") and projection ("Fig. 4(b)") are used in our method to assign one or more labels in each basin. We can observe that the sulcal projection shows several connected components and branches.

Indeed, several labels may be in the same basin. For instance, it is very common that the superior frontal sulcus and the precentral sulcus meet inside the same sulcal basin. On "Fig. 5(a)", these two sulci are including in the single yellow basin.

For this reason, we define a new set $B_{proj} \subset V$ as the result of a large dilation of the sulcal projection ("Fig. 5(b)").

We then define $B_{lab} = B_{proj} \cap B$ and label its connected components.

On "Fig. 4(a)" in green color, we can see that the superior frontal sulcus will be characterized in two distinct basins while it was used as a single connected component in the snake method [1].

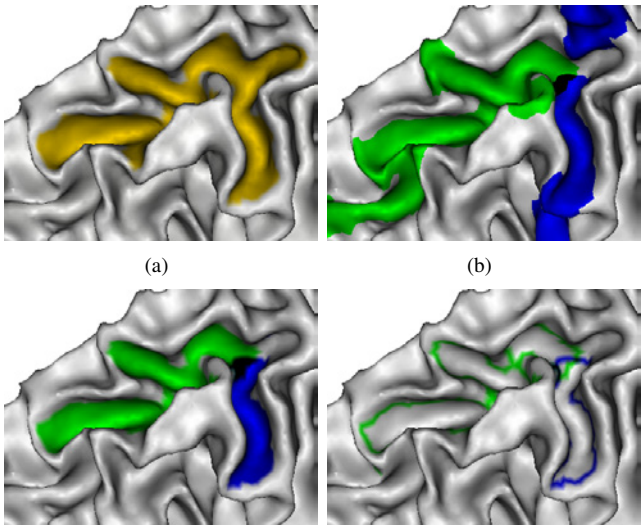

Fig. 5. (a) one labelled sulcal basin B (b) two projections closing with a larger structuring element B_{proj} (c) intersection $B_{lab} = B_{proj} \cap B$ (d) B_{cont} contour of B_{lab}

From these labeled basins, the main contribution of our method concerns calculating a path probability map. That is used to automatically find the extremities of the sulcal lines.

2) From path probability map to longest shortest path: We now consider the contour B_{cont} of B_{lab} (See "Fig. 5(d)"). On "Fig. 6(a)", some examples of distributed vertex belonging to the green contour of the blue basin show several paths (in red color) through this basin. For each pair of vertices $(v_i, v_j) \in B_{cont}$, we estimate the shortest path $S_{i,j}$ and we increment a counter on each vertex of the basin B_{lab} when it is crossed by S_{ij}.

This way, we define B_{proba} as the map of probability ("Fig. 6(b)") of belonging to a set sulcal lines, that we can normalize between 0 and 1 in each basin.

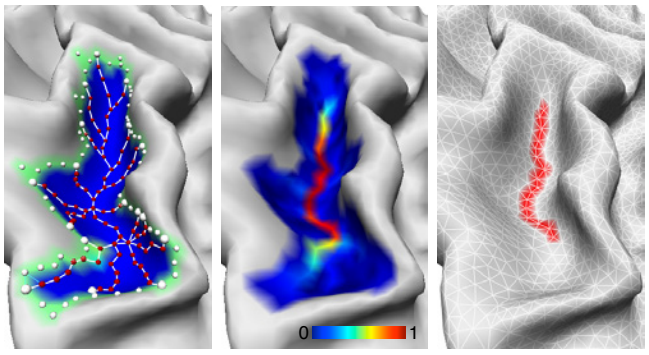

(a) (b) (c)

Fig. 6. (a) in green B_{cont}, in red a set of shortest paths $SP_{i,j}$ (b) path probability map B_{proba} from blue (0) to red (1) (c) longest shortest path LS

We threshold B_{proba} to keep only the points that have a high probability to belong to a sulcal lines. For this paper, the threshold was chosen empirically and fixed at 0.3. Let us denote $B_{thr} \subset B_{lab}$ this set. For each connected component $C_i \in B_{thr}$, we compute the longest shortest path LS_i between each vertex pair $(v_j, v_k) \in C_i$:

$$LS_i = \underset{\forall (v_j, v_k) \in C_i}{\arg\max} \{L(S_{jk})\} \quad (5)$$

LS_i is then taken as the sulcal line for the basin described by C_i.

III. RESULTS AND DISCUSSION

The performance of our method was evaluated on the left cortical surface of 20 subjects. Parameters were empirically set at $\lambda = 3$, $\gamma = 2$ and 0.3 as threshold of B_{proba} for all subjects. Two sulci (the central and frontal superior sulci) were manually delineated by an expert using the "surfpaint toolbox" [2] of Brainvisa software. We qualitatively and quantitatively compared our method with the sulcal projections from [10] and the snake algorithm [1]. We measured the deviation from the manually traced central sulcus (CS) and superior frontal sulcus (SFS) through the geodesic Hausdorff distance defined as follow. For two sets of vertices defining two sulcal lines P and Q,

$$d_{Hausdorff}(P, Q) = max\{d_{curv}(P, Q), d_{curv}(Q, P)\}$$

where

$$d_{curv}(P, Q) = \underset{i \in P}{sup}\ \underset{j \in Q}{inf}\ S_{ij}$$

The distribution of the Hausdorff distance through the 20 subjects for the three methods and the two sulci is shown on the "Fig. 7". This measure indicates a strong reduction of the deviation with our method as compared to others for both sulci (average for CS: our method 7.6, projections 20.6, snake 22.6 and for SFS: our method 11.9, projections 17.8, snake 20.0). Our approach clearly outperforms the two other methods.

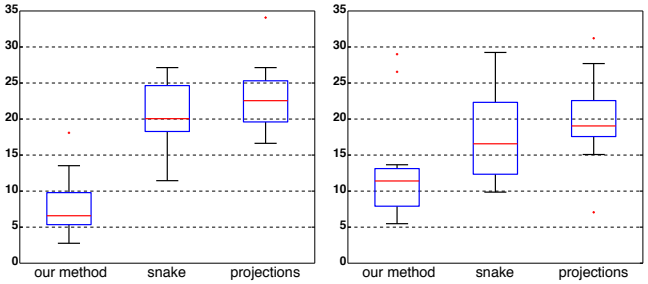

(a) Central sulcus (b) Superior frontal sulcus

Fig. 7. Descriptive statistics of geodesic Hausdorff distance, obtained for the three methods. For each box, the horizontal mark indicates the median value; the upper and lower edges contain the data distribution within the first lower through the last upper quartile values; the whiskers cover values within 1.5 times this interquartile range.

"Fig. 8" shows the results for the frontal superior sulcus obtained with our method. The snake algorithm reduces each sulcal projection into a single regular connected component. It is thus not designed to manage the multiple part sulci.

The superior frontal sulcus is often divided into two connected components separated by a gyrus. In this case, the major weakness of the snake method is that the sulcal line passes through the connecting gyrus ("Fig. 8(a)"), since the extremities of this curve are located in two separated basins. On "Fig. 8(b)", we show the result of our method in this configuration. The corresponding sulcal line is divided into two components (two sulcal lines having the same label), one in each basin.

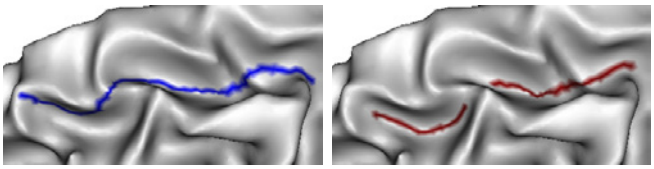

(a) snake method (b) our method

Fig. 8. Comparison of snake method (a) and our approach (b) for the frontal superior sulcus.

Moreover, our method deals with the extremities of sulci (the most variable part [13]) in a coherent manner. As shown on the "Fig. 9" with the lower extremity of the central sulcus, identifying the sulcal fundus is not clear in this region and two directions seem valuable. Indeed, the line traced by the expert is much shorter than the result from the snake. The expert chose to draw a short sulcal line instead of tracing a confusing part while the snake is constrained to choose one of the two branches. The path resulting from our method is very similar to the manually delineated line. This is the outcome of using probability maps as defined in section II-B.2, as illustrated on this figure. We show the probability map thresholded between 0.05 and 0.3. The potential branches appear in the probability map, with a low value (blue and cyan branches) and the final path corresponds to the vertices with a probability value greater than our threshold equal at 0.3, which results in an unambiguous short line.

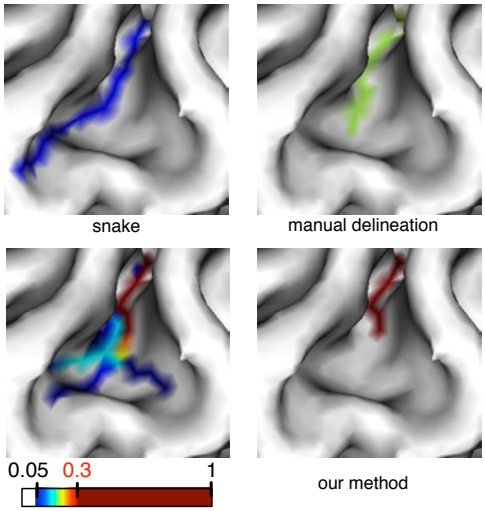

Fig. 9. Comparison of two methods snake and our method with manual delineation on the bottom region of central sulcus.

IV. CONCLUSION

In this paper, we proposed an automatic extraction of sulcal lines on the cortical surface using shortest path probability maps.

The method was applied to two major sulci, the superior frontal sulcus and the central sulcus. Results showed a good agreement with a manual segmentation and outperformed two other methods [1], [10]. The process should prove useful for methods using sulcal lines such as landmark based surface matching or sulcal morphometrics. Further work will evaluate performances on a lot more sulci and will focus on an automatic thresholding of the probability maps.

V. ACKNOWLEDGMENTS

Authors are funded by the Agence Nationale de la Recherche (ANR-09-BLAN-0038-01, 'Brainmorph')

REFERENCES

[1] C. Clouchoux, D. Rivière, J.F. Mangin, G. Operto, J. Régis and O. Coulon, "Model-driven parameterization of the cortical surface for localization and inter-subject matching", *in Neuroimage*, vol 50, no. 2, pp. 552-566, 2010.

[2] A. Le Troter, D. Rivière, and O. Coulon, "An interactive sulcal fundi editor in Brainvisa", *in Human Brain Mapping*, 2011.

[3] A. Bartesaghi, G. Sapiro, "A system for the generation of curves on 3D brain images", *in Human Brain Mapping*, vol. 14, no. 1, pp. 1-15, 2001.

[4] D.W. Shattuck, A.A. Joshi, D. Pantazis, E. Kan, R.A. Dutton, ER. Sowell, P.M. Thompson, A.W. Toga, R.M. Leahy, "Semi-automated method for delineation of landmarks on models of the cerebral cortex", *in Journal of Neuroscience Methods*, vol. 178, no. 2, pp. 385-392, 2008.

[5] J.K. Seong, K. Im, S.W. Yoo, S.W. Seo, D.L. Na, J.M. Lee, "Automatic extraction of sulcal lines on cortical surfaces based on anisotropic geodesic distance" *in Neuroimage*, vol 49, pp. 293-302, 2010.

[6] M.E. Rettmann, X. Han, C. Xu and J.L. Prince, "Automated sulcal segmentation using watersheds on the cortical surface", *in Neuroimage*,vol. 15, no. 2, pp. 329-344, 2002.

[7] Z. Tu, S. Zheng, A.L. Yuille, A.L. Reiss, R.A. Dutton, A.D. Lee, A.M. Galaburda, I. Dinov, P.M. Thompson, and A.W. Toga, "Automated Extraction of the Cortical Sulci Based on a Supervised Learning Approach", *in IEEE Transactions on Medical Imaging*, vol. 26, no. 4, pp. 541-552, 2007.

[8] Y. Shi, B. Sun, R. Lai, I. Dinov, A.W. Toga, "Automated Sulci Identification via Intrinsic Modeling of Cortical Anatomy", *in Med Image Comput Comput Assist Interv.*, vol.13 pp. 49-56, 2010.

[9] D. Rivière, J.F. Mangin, D. Papadopoulos-Orfanos, J.M. Martinez, V. Frouin, J. Régis, "Automatic recognition of cortical sulci of the human brain using a congregation of neural networks", in Medical Image Analysis, vol. 6, no. 2, pp. 77-92, 2002.

[10] A. Cachia, J.F. Mangin, D. Rivière, D. Papadopoulos-Orfanos, F. Kherif, I. Bloch, J. Régis, "A generic framework for parcellation of the cortical surface into gyri using geodesic Voronoi diagrams", *in Medical Image Analysis*, vol. 7, no. 4, pp. 403-416, 2003.

[11] E.W. Dijkstra, "A note on two problems in connexion with graphs", *in Numerische Mathematik*, vol. 1, pp. 269–27, 1959.

[12] V. Surazhsky, T. Surazhsky, D. Kirsanov, S.J. Gortler, and H. Hoppe, "Fast exact and approximate geodesics on meshes", *in ACM Transactions on Graphics*, vol. 24, no. 3, pp. 553-560, 2005.

[13] S. Durrleman, X. Pennec, A. Trouvé, P. Thompson, N. Ayache, "Inferring Brain Variability from Diffeomorphic Deformations of Currents: an integrative approach", *in Medical Image Analysis*, vol. 12, no. 5, pp. 626-637, 2008.